Nuclear Instruments and Methods in Physics Research B 295 (2013) 99–106

Contents lists available at SciVerse ScienceDirect

Nuclear Instruments and Methods in Physics Research B

journal homepage: www.elsevier.com/locate/nimb

Numerical calculations of cosmic ray cascade in the Earth's atmosphere – Results for nucleon spectra

Aleksandr Nesterenok *

Ioffe Physical-Technical Institute, 26 Polytechnicheskaya St., 194021 Saint Petersburg, Russia
St. Petersburg State Polytechnic University, 29 Polytechnicheskaya St., 195251 Saint Petersburg, Russia

ARTICLE INFO

Article history:
Received 22 August 2012
Received in revised form 7 November 2012
Available online 5 December 2012

Keywords:
Cosmic rays
Earth's atmosphere
Nucleon flux
Cosmogenic nuclides

ABSTRACT

The interaction of primary cosmic rays with Earth's atmosphere is investigated using the simulation toolkit Geant4. The yield functions of atmospheric nucleon fluxes are computed for the energy of primary cosmic ray particles ranging from 0.1 to 10^4 GeV. The model is presented that enables to calculate differential particle fluxes in the atmosphere for given level of solar modulation and geomagnetic latitude. The accuracy of the computations is verified by experimental data taken under various conditions. The calculated particle fluxes can be employed for estimation of the production rates of cosmogenic nuclides in the atmosphere and Earth's surface, for calculations of cosmic ray exposure dose for the public and soft-error failure rates in the microelectronics.

1. Introduction

The Earth's atmosphere is permanently bombarded by energetic particles of cosmic rays and a cascade of secondary particles is produced. It is essential to know the temporal and spatial variation of cosmic ray particle fluxes in the atmosphere for many geophysical and engineering problems such as production of cosmogenic nuclides, radiation dosimetry and single event upsets in the microelectronics [1–3].

Galactic cosmic rays are affected in the heliosphere by the interplanetary magnetic field and solar wind. The varying magnetic field carried outward from the sun by the solar wind plasma deflects incoming galactic cosmic rays and reduces the particle flux. Solar modulation is the dominant cause of the galactic cosmic ray variability near the Earth. The magnetic field of the Earth also acts as a shield. Depending on the geomagnetic latitude and angle of incidence, there is a critical energy below which cosmic ray particles cannot penetrate into the Earth's atmosphere. As a result the latitudinal dependence of the primary particle fluxes is observed [4]. The cosmic ray particles interact by electromagnetic and nuclear processes with the atoms of the Earth's atmosphere and produce secondary particles. Particles are generated by successive interactions of the primary or of the secondary particles and thus form a cascade in the atmosphere. Some of the particles produced in the cascade can reach the Earth's surface and induce nuclear reactions there.

To quantify the effect of cosmic rays on the Earth's environment it is important to know precisely the flux of cosmic ray shower particles in function of position, atmospheric depth, and time. A number of studies have been devoted to the calculation of cosmic ray particle spectra in the atmosphere. The most of the earlier work was based on the solution of transport equations [5]. Particles of the same species in the cascade initiated by primary cosmic-ray particles are treated collectively as distributions. The transport equations represent the rule which connects the changes between the particle distributions as they are propagating in the atmosphere. An alternative approach to the treatment of atmospheric particle cascade is the Monte Carlo calculations [1,2,6–18]. The trajectories of all the particles in the cascade are simulated until they are absorbed by nuclei, stopped or escape from the atmosphere. Numerical or Monte Carlo calculations are needed to account accurately for decay and energy-loss processes, and for the energy-dependence of the cross sections.

The shape of the galactic cosmic ray spectrum is often prescribed in the numerical models [1,2,7–13]. But the fluxes of primary cosmic radiation at the top of the atmosphere depend on location in the geomagnetic field and solar magnetic activity. It is time consuming to perform numerical simulations of the cosmic ray propagation for each set of geophysical parameters. The rapid calculation of atmospheric particle fluxes is required in some problems such as evaluation of aviation doses [11,12]. Based on the Monte Carlo simulations, an analytical model is proposed in Refs. [11,12] for estimating cosmic ray particle fluxes in the atmosphere applicable to any global conditions. Another approach to the rapid flux calculations consists in simulating of cosmic ray particle cascade initiated by the primary particle of the given type and fixed

* Tel: +7 812 292 71 80; fax: +7 812 5504890/2971017.
E-mail address: alex-n10@yandex.ru

0168-583X/$ - see front matter © 2012 Elsevier B.V. All rights reserved.
http://dx.doi.org/10.1016/j.nimb.2012.11.005

energy with the results being stored separately for each primary energy and type. As a result the yield functions of secondary particle fluxes are computed that can be convoluted with a given energy spectrum of the primary cosmic rays. This approach has been used in Refs. [14–17] and the models have been suggested for calculation of the cosmic ray induced ionization and cosmogenic nuclide production rates in the atmosphere. We adopt this approach for the simulation of cosmic ray particle cascade in the Earth's atmosphere. The aim of this study is to provide a model for rapid calculation of cosmic ray particle spectra in the atmosphere for any given set of geophysical parameters.

2. Calculational model

2.1. Physics input

Particle fluxes in matter are calculated using simulation toolkit Geant4 9.5 patch-01 [19]. The processes included are those of production, propagation and interaction of baryons (nucleons, short-lived baryons and their antiparticles), mesons (pions and kaons), light nuclei, leptons (electrons, positrons, muons) and gamma rays. Standard electromagnetic processes, photonuclear and electronuclear processes are taken into account [20]. Particles of electron–photon component with energies less than 10 MeV are excluded from calculations. Fritiof Precompound model is employed to describe inelastic scattering of hadrons and nuclei at high energies. Note that the Fritiof Precompound model is capable to treat inelastic scattering of nuclei projectiles in the current version of Geant4. The Bertini intranuclear cascade model is employed for describing nucleon–nucleus and meson–nucleus inelastic scattering at hadron energies up to 10 GeV. The binary intranuclear cascade model and quantum molecular dynamics model are adopted for inelastic scattering of light nuclei at energies up to 10 GeV. The intranuclear cascade models are used in conjunction with precompound deexitation model. Processes of negative meson capture, neutron capture and neutron fission are included. High precision neutron models are used for simulating neutron–nucleus interactions at neutron energies below 20 MeV. These models are based on the G4NDL data library (version 4.0) that comes largely from the ENDF-B VII and JENDL libraries. At neutron energies in the range from 20 MeV to about 3 GeV the JENDL/HE cross section data are employed.

2.2. Model of the Earth's atmosphere and surface

The Earth is modelled as a sphere of a radius of 6371 km. The elemental composition of the surface is assumed to be an average composition of the upper continental crust – in weight percents, 46% O, 34% Si, 8.2% Al, 3.5% Fe, 2.6% Ca, 2.4% Na, 2.3% K, 1.5% Mg [21]. The surface density is taken to be 2.65 g/cm^2.

The atmosphere is considered as a spherical shell of 100 km thickness. The chemical composition of the air (by mass) is nitrogen 75.5%, oxygen 23.2% and argon 1.3%. The total thickness of the atmosphere is taken to be equal to the atmospheric depth of 1034 g/cm^2 at sea level. The atmosphere is divided into concentric subshells with a thickness of 15 g/cm^2 and constant air density within one subshell. Additional division is done near air-ground interface. The dependences of air density and temperature on altitude are taken from the COSPAR reference atmosphere data [22]. The data are averaged over the latitude.

The atmospheric shielding from the cosmic ray particle flux at a given altitude is determined by the mass of atmosphere traversed by the particles. To apply simulation results to a given location on the Earth one needs to convert site altitude to atmospheric depth using pressure data or appropriate air density dependence on altitude.

2.3. Geomagnetic field

The cosmic ray particles are affected by the terrestrial geomagnetic field. The geomagnetic field inhibits low-energy charged primaries from penetrating the atmosphere for equatorial and mid-latitude positions. Depending on the field strength and angle of incidence there is a rigidity (the particle momentum per unit charge) above which all charged particles are allowed – upper cutoff value; and there is a rigidity below which all charged particles are forbidden – lower cutoff value. Between the upper and lower cutoff values there is a chaotic region of allowed and forbidden trajectories – cosmic ray penumbra [23,24]. "Effective" geomagnetic cutoff rigidity for a given direction can be introduced. The effective geomagnetic cutoff rigidities in vertical direction are used as an approximation of the cutoff parameters in some numerical models [14–17]. In the majority of cases the effective vertical geomagnetic cutoff is a sufficiently good approximation [25]. Values of effective vertical geomagnetic cutoff rigidity have been calculated by Shea and Smart [24] for a grid of locations covering the globe. The parameter is near zero at the poles and has a maximum of about 15–17 GV at the equator.

2.4. Calculation of particle fluxes

The energy range of the spectrum of primary particles is split into intervals. The number of energy intervals is taken to be 16 in the energy ranges 1–10, 10–10^2 GeV/nucleon and is taken to be 8 in the energy ranges 0.1–1, 10^2–10^3, 10^3–10^4 GeV/nucleon. The simulation of particle cascade in matter initiated by the primary particle of a given type is performed with results being stored separately for each energy interval of the primary. Within each interval the primary energy is sampled at random for energies up to 10 GeV/nucleon and is sampled according to power spectrum with the exponent −2.7 for higher energies. The particle distribution over the nadir angle θ is adopted to be proportional to $\cos\theta\sin\theta$ with the nadir angle being sampled in the range 0–90°. We consider two most abundant species of galactic cosmic rays – protons and α-particles. We consider primary particles with energies up to 10 TeV for protons and up to 3 TeV/nucleon for α-particles.

Directed differential flux of particles k in matter at a depth z initiated by primary particles i with energy E is calculated according to:

$$J^{\mathrm{diff}}_{k,i}(z,\varepsilon,o,E)=\frac{1}{N_i\Delta\varepsilon\Delta o}\sum_{z,\Delta\varepsilon,\Delta o}\frac{1}{|\cos\theta_k|}, \quad (1)$$

where ε – particle energy, o – momentum direction, N_i is the number of primary particles (protons or α-particles) for which the cascade simulations are performed, θ_k is the particle nadir angle, the summation is done over all particles k crossing a fixed level in matter at depth z and having energies in the range $(\varepsilon-\Delta\varepsilon/2,\ \varepsilon+\Delta\varepsilon/2)$ and momentum direction in the solid angle Δo. The particle fluxes are calculated as a function of nadir angle θ. The nadir angle range is split into intervals of length 15° for angles less than 90° and one interval 90–180° is considered. The Eq. (1) is normalized to unit flux of the primary particles impinging on the top of the atmosphere.

Eq. (1) represents the yield functions of particle fluxes which can be convoluted with a given spectrum of primary particles. Different types and approximations of energy spectra of primary particles can be used that constitutes the flexibility of the approach. The differential flux of particles k in matter initiated by primary particles i with a given spectrum can be computed as:

$$J^{\mathrm{diff}}_{k,i}(z,\varepsilon,o) = \pi \int_{E_{ic}}^{\infty} dE J^{\mathrm{diff}}_{k,i}(z,\varepsilon,o,E)\cdot J^{\mathrm{diff}}_{i}(E), \quad (2)$$

where $J^{\mathrm{diff}}_{i}(E)$ is the directed differential flux of primary cosmic ray nuclei of type i near the Earth's orbit, E_{ic} – particle energy corresponding to geomagnetic cutoff of the spectrum. The angle dependence of the effective geomagnetic cutoff rigidity is not taken into account in the Eq. (2). Vertical or apparent geomagnetic cutoff values can be used in calculations as an approximation of geomagnetic cutoff of primary particle spectra.

The Z/A ratio determines the shape of the differential energy spectrum modulated in the heliosphere (see next section). This ratio is close to 1/2 for nuclei with charge numbers $Z \geqslant 2$. Heavy nuclei have roughly the same rigidity as α-particles with the same energy per nucleon. Hence, the behavior of nuclei $Z \geqslant 2$ in the geomagnetic field is expected to be similar. The species of galactic cosmic rays heavier than α-particles can be considered as additional α-particles. The contribution of all $Z \geqslant 2$ nuclei to particle cascade in matter is determined by applying a scaling factor f to the results, obtained for α-particles. This scaling factor is the ratio of nucleon number densities of all $Z \geqslant 2$ nuclei to α-particles in the galactic cosmic rays. The data on relative abundance of cosmic-ray nuclei are used from the Refs. [26,27] and the value of $f = 1.4$ is evaluated. The total differential flux of particles k in matter can be calculated as:

$$J^{\mathrm{diff}}_{k}(z,\varepsilon,o) = J^{\mathrm{diff}}_{k,p}(z,\varepsilon,o) + 1.4 \times J^{\mathrm{diff}}_{k,\alpha}(z,\varepsilon,o),$$

where subscript p corresponds to primary protons and subscript α – to primary α-particles. The angle-integrated differential particle flux can be computed according to:

$$I^{\mathrm{diff}}_{k}(z,\varepsilon) = \int_{4\pi} do J^{\mathrm{diff}}_{k}(z,\varepsilon,o).$$

The directed integral particle flux and the angle-integrated integral particle flux are calculated as:

$$J^{\mathrm{int}}_{k}(z,o) = \int_{\varepsilon_1}^{\varepsilon_2} d\varepsilon J^{\mathrm{diff}}_{k}(z,\varepsilon,o),$$

$$I^{\mathrm{int}}_{k}(z) = \int_{\varepsilon_1}^{\varepsilon_2} d\varepsilon I^{\mathrm{diff}}_{k}(z,\varepsilon),$$

where $(\varepsilon_1, \varepsilon_2)$ is a given energy interval.

The total number of primary particles for which the cascade simulations are performed is 7.5 million for protons and 2.5 million for α-particles. Simulations have been performed at the Saint-Petersburg branch of Joint Supercomputer Center of the Russian Academy of Sciences. It takes about 5 days to run the simulations on 100 processor cores of 12 GFlops performance each one. The calculated yield functions of nucleon directed differential fluxes and the C++ code necessary for calculation of atmospheric particle fluxes are available in the internet at http://www.github.com (repository name "Numerical_calculations_of_cosmic_ray_cascade") and can be sent by e-mail upon request.

2.5. The spectra of primary cosmic rays near the Earth's orbit

Primary cosmic rays at energies above several hundred MeV per nucleon are mostly of galactic origin, about 90% of particles being protons and 10% helium nuclei. The particle fraction of heavier nuclei does not exceed 1%. At energies below few GeV per nucleon the flux of galactic cosmic rays in space at the Earth's orbit significantly depends on the level of solar activity. In the force field model the level of the solar modulation of particle spectra is described by the modulation potential, which characterizes the energy losses of cosmic rays in the heliosphere. The differential energy spectrum of cosmic ray nuclei of type i in the force field approximation is given by [28]:

$$J^{\mathrm{diff}}_{i}(E) = J_{LIS,i}(E+\Phi_i)\frac{E(E+2m_pc^2)}{(E+\Phi_i)(E+\Phi_i+2m_pc^2)}, \quad (3)$$

where $J_{i,LIS}(E)$ gives the local interstellar spectrum of nuclei i, E is nucleus kinetic energy per nucleon, m_pc^2 is proton's rest-mass energy, $\Phi_i = (eZ_i/A_i)\phi$, Z_i and A_i are nucleus charge and mass numbers, respectively, e is the elementary charge, and φ is the modulation potential which is related to solar activity. There are several models of the local interstellar spectrum [29,30]. However, despite the differences all the models of local interstellar spectrum allow a parameterization of the modulated spectra in the vicinity of the Earth [29,30]. We take the parameterization of the local interstellar spectrum from the Refs. [30,31]:

$$J_{i,LIS}(E) = C_i \frac{p(E)^{-2.78}}{1+0.487p(E)^{-2.51}},$$

where E is expressed in GeV per nucleon, $p(E) = \sqrt{E(E+2m_pc^2)}$, C_i is the normalization factor; $C_p = 1.9\ 10^4$ (m^2 s sr GeV)$^{-1}$ for protons, and $C_{He} = 9.5\ 10^2$ (m^2 s sr GeV/nucleon)$^{-1}$ for helium nuclei. The values of the modulation potential of galactic cosmic rays are reconstructed for the last half-century in Refs. [30,32] based on the data of ground-based neutron monitors and ionization chambers. The reconstructed annual values of the modulation potential φ range from 0.3 GV to 1.2 GV. The value of modulation potential of 0.65 GV is adopted in this study as an average value for the present epoch [32]. Note that the exact value of the modulation potential describing the given spectrum depends on the model of local interstellar spectrum used [29,30].

The power functions for the primary particle spectra are employed for energies higher than 100 GeV:

$$J^{\mathrm{diff}}_{i}(E) = A_i E^{-\gamma_i}, \quad (4)$$

where particle energy E is expressed in GeV/nucleon, parameters A_i and γ_i for protons and helium nuclei are taken according to the results of ATIC2 experiment [33]. Primary particle differential energy spectra (3) and (4) are substituted into the Eq. (2) to calculate particle fluxes in the atmosphere.

The energetic particles from the Sun are mostly protons and have energies up to few GeV. Solar events producing protons with energies above 1 GeV are rare [1,4]. Some solar particle events have proton fluxes much higher than average and could make contribution to the particle fluxes in the atmosphere [1]. To study this phenomenon, the spectrum of solar energetic particles has to be taken into account in the Eq. (2). The long-term average flux of solar protons is not expected to make significant contribution to cascade processes in the atmosphere [1,4]. We don't consider solar cosmic ray particles in the calculations.

3. Results and discussion

3.1. Integral fluxes of cosmic ray nucleons in the atmosphere

Fig. 1 shows the depth dependence of the angle-integrated integral fluxes of protons and high energy neutrons in the Earth atmosphere. Neutrons with energies higher than 10 MeV are considered. The solar modulation parameter value of 0.65 GV is used and four values of geomagnetic cutoff R_C are taken in the computation – 0 GV, 4 GV, 9 GV and 14 GV. Statistical errors of the calculated fluxes are on the level of 1–2% at sea level and lower for higher altitudes. Neutron flux has a broad maximum in the depth interval 30–150 g/cm^2. At atmospheric depth exceeding about 200 g/cm^2, neutron flux decreases roughly exponentially with increasing depth. The effective attenuation length of cosmic ray neutron flux in the atmosphere varies with altitude and location in the geomagnetic field. For altitudes below 4 km (atmospheric

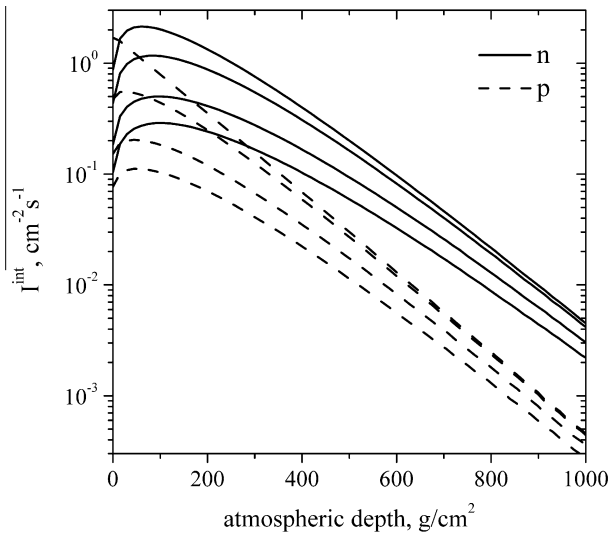

Fig. 1. The depth dependence of the angle-integrated integral fluxes of protons and high energy neutrons in the Earth atmosphere. Solid line is for neutrons, dashed line is for protons. Four values of the geomagnetic cutoff parameter R_C are adopted – from top to bottom – 0 GV, 4 GV, 9 GV and 14 GV.

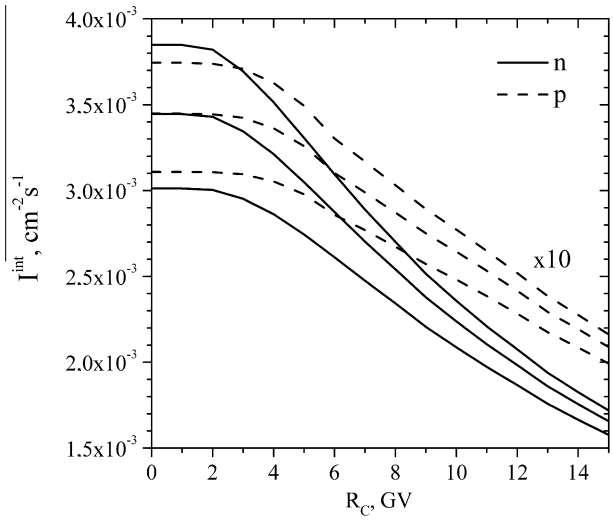

Fig. 2. The geomagnetic cutoff distribution of the angle-integrated integral fluxes of protons and high energy neutrons at sea level. Solid line is for neutrons, dashed line is for protons. The solar modulation parameter is taken to be – from top to bottom – 0.4 GV, 0.65 GV and 1 GV. The proton flux values are multiplied by 10.

depths larger than 630 g/cm^2) the effective attenuation length of high energy neutron flux is found to be 130 g/cm^2 at high geomagnetic latitudes and 148 g/cm^2 at geomagnetic cutoff R_C = 14 GV. Statistical errors of the parameter are less than 1%. The compilation of neutron monitor network data provides a value for the effective attenuation length of high energy nucleon flux of 130 g/cm^2 at high geomagnetic latitudes and of 145–150 g/cm^2 at equatorial regions [34–36]. According to our calculations, the relative contribution of protons to the high energy nucleon flux is about 10–12% at sea level.

Fig. 2 presents the geomagnetic cutoff distribution of the angle-integrated integral fluxes of protons and high energy neutrons at sea level. Neutrons with energies higher than 10 MeV are considered. The solar modulation parameter is chosen to be 0.4 GV, 0.65 GV and 1 GV which are representative values for the periods of minimum, medium and maximum of solar activity, respectively. The ratio of the high energy neutron flux at sea level at cutoff rigidity R_C = 14 GV to that at R_C = 0 GV is found to be 0.47, 0.51 and 0.55 for low, average and high levels of solar activity, respectively. The sea level latitude effect for protons is found to be 0.61, 0.64 and 0.67 at the same geomagnetic cutoff rigidities and for the levels of solar activity in question, respectively. Note that the neutron and proton fluxes are found to have different geomagnetic cutoff distributions. The latitude effect is found to be more pronounced for neutron flux than for proton flux. The proton fluxes are less affected by the changes in the solar activity level than neutron fluxes. It may be attributed by the fact that the relative contribution of high energy primaries to the proton flux formation is higher than in the case of neutrons. The calculated results are consistent within 10% with the data of latitude surveys conducted with the neutron monitors [35].

The contribution of particle cascades initiated by nuclei Z $\geqslant$ 2 of galactic cosmic rays to the nucleon fluxes in the lower atmosphere is found to be 36–38% for high geomagnetic latitudes and 40–43% near the equator.

3.2. Differential fluxes of cosmic ray nucleons in the atmosphere

Fig. 3 shows calculated neutron angle-integrated differential flux at the atmosphere-ground interface at sea level. The modulation potential value of 0.65 GV is taken in calculation. For comparison, we present the neutron angle-integrated differential fluxes from the Refs. [8,11,37,38]. The differential flux from the Ref. [37] represents a fit through previously published experimental data. The spectrum is adjusted to sea level and New York City geomagnetic latitude. The data from the Ref. [38] are the results of neutron spectrum measurements scaled to sea level high geomagnetic latitudes and mean level of solar modulation. Gordon et al. [38] estimate the uncertainty in the response functions for the detectors to be 10–15% above 150 MeV and lower for lower energies, producing a similar uncertainty of the measured data. The data from the Ref. [11] are the results of Monte Carlo simulations using the PHITS code coupled with the nuclear data library JENDL/HE. The spectrum was calculated for semi-infinite atmosphere without considering air-ground interface. The neutron

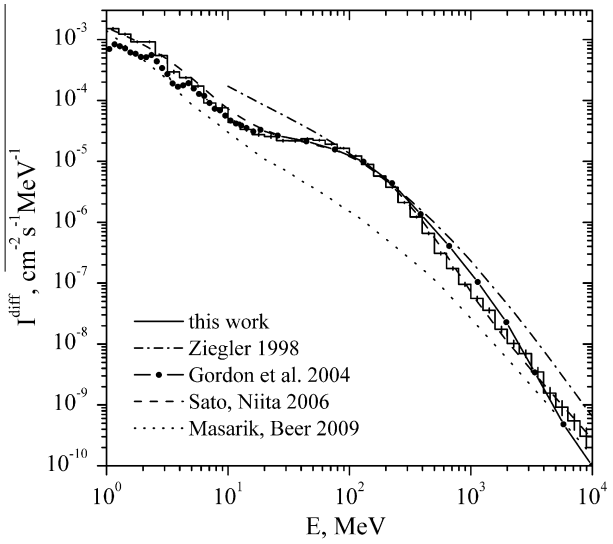

Fig. 3. The neutron angle-integrated differential flux at the atmosphere-ground interface. Step-like curve shows calculated results, error bars show statistical uncertainty. Dash-dot line is for the spectrum from the Ref. [37]. Circles connected by line present measured spectrum [38]. Dashed line is for computed spectrum from the Ref. [11], dot line – calculated spectrum from the Ref. [8].

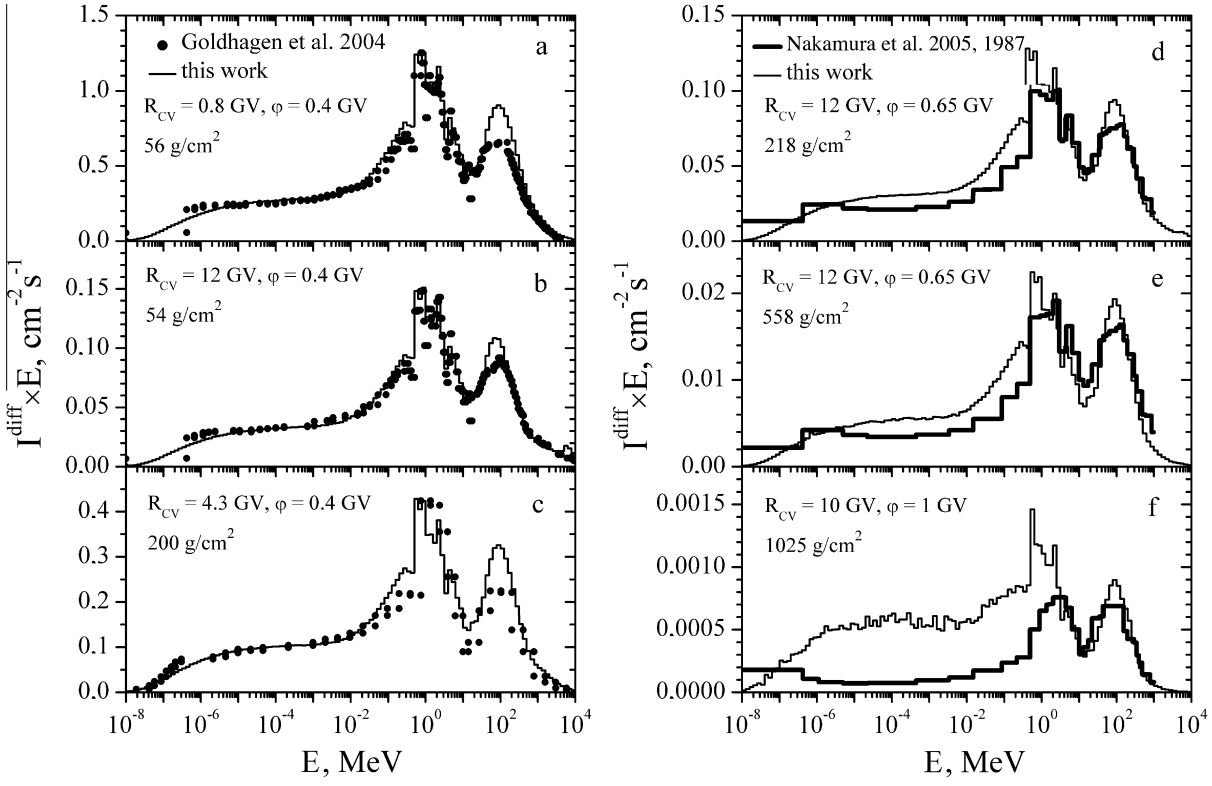

Fig. 4. The neutron angle-integrated differential flux in the atmosphere. The graphs show spectra for different geographic locations and solar modulation. The experimental data are taken from the Ref. [39] – graphs a, b, c – and from the Ref. [40,41] – graphs d, e, f. Thin step-like curve presents calculated results. The values of solar modulation parameter φ, vertical geomagnetic cutoff rigidity R_{CV} and atmospheric depth are specified in the plots.

differential flux from the Ref. [8] represents the results of Monte Carlo simulations using the Geant4 and MCNP code systems.

Ground level neutron flux depends strongly on the landscape geometry and the chemical composition of the ground [9,11]. There is significant dependence of the neutron spectrum at low energies on the weight fraction of hydrogen or water in the ground, the neutron fluxes being lower for higher hydrogen content [9,11]. The hydrogen is not included in the ground composition in our simulations. The differences between calculated and measured neutron spectra at energies below few MeV may be attributed to the air-ground interface effects.

There is agreement between the neutron differential flux calculated in this work and the flux calculated in the Ref. [11]. On the contrary, there is substantial disagreement between neutron differential flux obtained in this work and the one from the Ref. [8] despite the fact, that the Geant4 code system is used in both simulations. The discrepancy in the spectra may be suggested as arising from different physical models and cross section data used in the simulations.

Fig. 4 shows the measured and calculated neutron angle-integrated differential fluxes for different atmospheric depths, geomagnetic cutoffs and solar modulation. The experimental data are taken from the Refs. [39–41]. The neutron flux values multiplied by neutron energy are plotted in the vertical axis with a logarithmic scale on the horizontal axis. In calculations, the values of the solar modulation parameter correspond to the date of measurements. The parameter value is adopted according to the results of the Ref. [32]. The effective vertical geomagnetic cutoff rigidities are used in calculations. There is good agreement between measured and calculated atmospheric neutron fluxes at energies up to 10 MeV. The large discrepancy between calculated and measured fluxes at the ground level can be accounted for by the difference in the ground composition at the measurement site and that

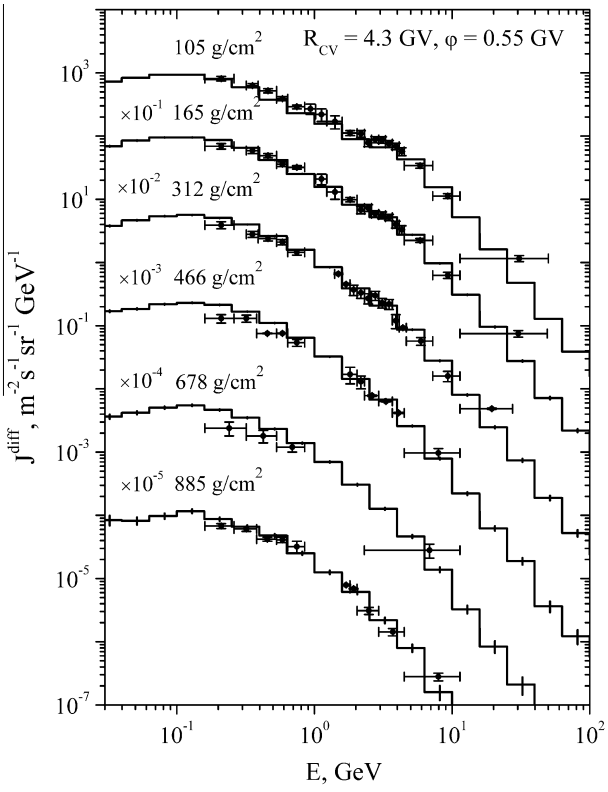

Fig. 5. The proton differential flux in vertical direction at different atmospheric depths. Step-like curve shows calculated results, error bars show statistical uncertainty. Circles with error bars present measured spectrum [42].

adopted in the simulations. The measured and calculated fluxes agree within 30% at neutron energies 10–300 MeV corresponding to the high energy peak of neutron energy spectrum. The shape of neutron energy spectrum does not change significantly with altitude, geomagnetic cutoff, or solar modulation except for the air-ground interface region.

Fig. 5 presents the proton differential flux in vertical direction at various altitudes in the atmosphere. The experimental data are taken from the Ref. [42]. The measurements were made at a vertical rigidity cutoff of about 4.3 GV. The modulation potential value of 0.55 GV is taken in computation. There is a reasonable agreement between measured and calculated spectra at all altitudes.

3.3. Angle distribution of nucleon fluxes in the atmosphere

Fig. 6 presents the integral particle fluxes as a function of nadir angle for various atmospheric depths. The average value of solar modulation parameter is considered. At the top of the atmosphere the neutron flux has non-zero values only for nadir angles in the range 90–180° illustrating the neutron leakage out from the atmosphere. The angle distributions of high energy particle fluxes become peaked in the vertical direction at high atmospheric depth. While the fluxes of low energy neutrons are isotropic and do not depend on angle. The angular distribution of high energy cosmic ray nucleons can be presented as:

$$J(\theta) = J_0 \exp[\alpha(1 - \cos\theta)],$$

where J_0 is the particle flux in the vertical direction, θ is the particle nadir angle, here $0 < \theta < 90°$. For the nucleons with energies higher than 10 MeV and high geomagnetic latitudes, our calculations give $\alpha = -1.8 \pm 0.1$ and $\alpha = -2.5 \pm 0.1$ for atmospheric depths 300 g/cm^2 and 990 g/cm^2, respectively. Angle distributions of particle fluxes become more peaked in the vertical direction at depth closer to the Earth's surface. The correction factors accounting for the shielding of the nucleonic component of the cosmic radiation at the Earth's surface due to surrounding topography can be calculated based on the computed angle distributions of particle fluxes.

3.4. The cosmic ray particle cascade production in the atmosphere

We have studied the relative contribution of the galactic cosmic ray particles to the secondary particle cascade formation in the atmosphere. Fig. 7 shows the energy dependence of primary particle contribution to the nucleon flux in the atmosphere at a depth 60 g/cm^2. The average value of solar modulation parameter and the high geomagnetic latitudes are considered in computation. The nucleons of all energies are considered. The nucleon angle-integrated integral fluxes induced by primary protons and α-particles are found to be 6.5 cm^{-2} s^{-1} and 1.9 cm^{-2} s^{-1} at atmospheric depth in question, respectively. The energies of primary particles that provide the 66% contribution to the nucleon fluxes are found

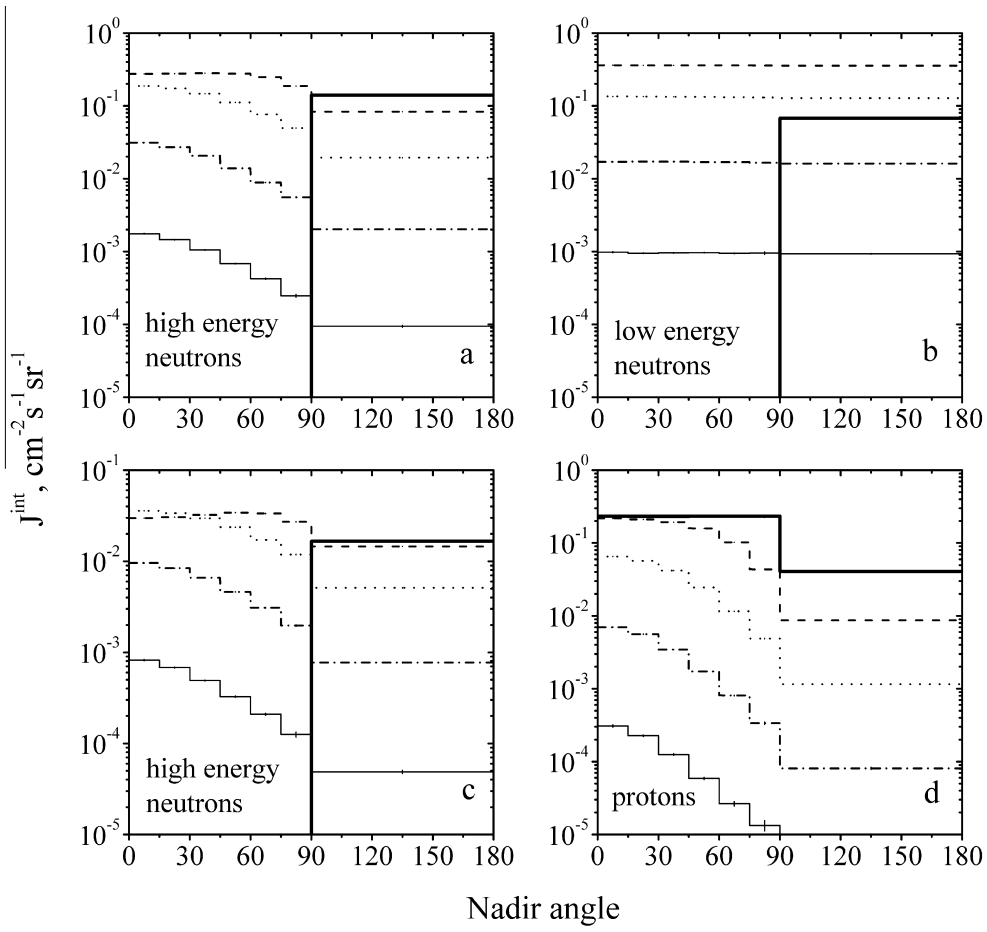

Fig. 6. Neutron and proton fluxes in the atmosphere as a function of the nadir angle. The *y*-axis shows the particle directed integral flux. The fluxes of high energy neutrons (with energies higher than 10 MeV) at geomagnetic cutoff rigidity 0 GV are illustrated in the graph a. The fluxes of neutrons with energies lower than 1 MeV at geomagnetic cutoff rigidity 0 GV are illustrated in the graph b. The graph c shows high energy neutron fluxes at geomagnetic cutoff rigidity 14 GV. The angle distribution of proton fluxes at geomagnetic cutoff rigidity 0 GV are presented in the graph d. Thick solid line corresponds to the top of the atmosphere, dashed line is for atmospheric depth 90 g/cm^2, dot line is for 300 g/cm^2, dash-dot line – 600 g/cm^2, thin solid line – 990 g/cm^2.

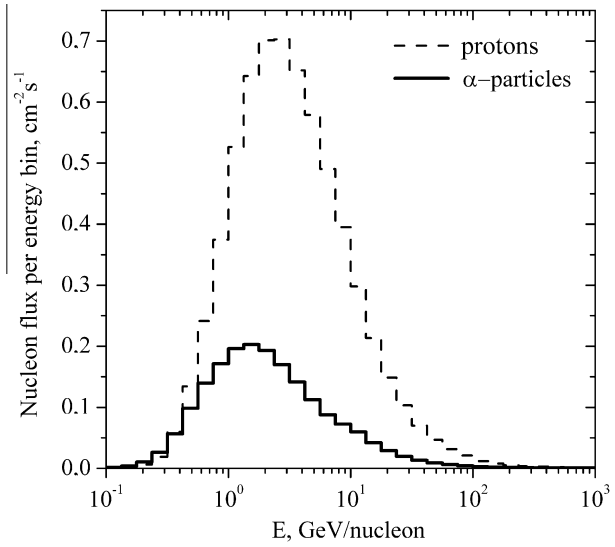

Fig. 7. The energy dependence of primary particle contribution to the nucleon flux in the atmosphere. The *y*-axis shows the nucleon angle-integrated integral flux per energy bin of primary particles. Solid line is for primary α-particles, dashed line is for primary protons. The atmospheric depth is 60 g/cm^2.

in the range 1–7.5 GeV for primary protons and 0.6–5 GeV/nucleon for primary α-particles. The energies of primary particles responsible to secondary particle flux formation become higher with increasing atmospheric depth and are estimated to be in the range 3–30 GeV for protons and 2–20 GeV/nucleon for α-particles at sea level. The primary particle spectra have to be determined accurately at these energy regions. The contribution of primary particles with energies higher than 100 GeV/nucleon to nucleon fluxes is lower than 1% at low atmospheric depth and about 6–7% at sea level.

4. Conclusions

The model is presented for calculation of cosmic ray particle fluxes in the Earth's atmosphere. The cosmic ray particle cascade initiated by the primary particle of the given type and fixed energy is simulated using the toolkit Geant4 and the results are stored separately for each particle type and energy. The calculated yield functions of particle fluxes are convoluted with the primary cosmic ray spectra and nucleon fluxes in the atmosphere are computed. The neutron and proton energy spectra are calculated as a function of nadir angle. The approach used in the work enables to calculate differential particle fluxes at various geophysical conditions without performing full Monte Carlo simulations. The simulations corresponding to a given energy and type of primary particle can be compared with other analogous simulations where different physical models are employed. This can facilitate the understanding of possible discrepancies between the results of various numerical models.

The angle-integrated integral fluxes of protons and high energy neutrons in the atmosphere are considered. The calculated effective attenuation length of high energy neutron flux agrees with the data of neutron monitors. The geomagnetic cutoff distributions of nucleon fluxes in the atmosphere are calculated. The latitude effect is found to be more pronounced for neutron flux than for proton flux. A comparison is made between calculated differential particle fluxes in the atmosphere and experimental data taken under various conditions. The calculated particle fluxes are in a reasonable agreement with the experimental data. The relative contribution of the primary cosmic ray particles to the particle cascade formation in the atmosphere is investigated. The energies of primary particles that give the main contribution to the nucleon fluxes in the atmosphere are calculated.

The model presented enables to calculate the energy spectra of protons and neutrons with a sufficiently good precision both for high geomagnetic latitudes and for equatorial regions. The results of the work can be used in the studies of cosmogenic nuclides produced in the atmosphere and terrestrial rocks as well as in the calculations of cosmic ray exposure dose for the public and soft-error failure rates in the microelectronics.

Acknowledgements

I am very grateful to my supervisor Victor O. Naidenov for teaching and helping me. This work was supported by Ministry of Education and Science of Russian Federation (Contract # 11.G34.31.0001 with SPbSPU and leading scientist G.G. Pavlov and Agreement No. 8409, 2012).

References

[1] J. Masarik, R.C. Reedy, Terrestrial cosmogenic-nuclide production systematics calculated from numerical simulations, Earth Planet. Sci. Lett. 136 (1995) 381–395.
[2] S. Roesler, W. Heinrich, H. Schraube, Monte Carlo calculation of the radiation field at aircraft altitudes, Radiat. Prot. Dosim. 98 (2002) 367–388.
[3] H.H.K. Tang, K.P. Rodbell, Single-event upsets in microelectronics: fundamental physics and issues, MRS Bull. 28 (2003) 111–116.
[4] K. Scherer, H. Fichtner, T. Borrmann, et al., Interstellar-Terrestrial Relations: Variable Cosmic Environments, The Dynamic Heliosphere, and Their Imprints on Terrestrial Archives and Climate, Space Sci. Rev. 127 (2006) 327–465.
[5] K. O'Brien, Cosmic-ray propagation in the atmosphere, Nuovo Cimento A Ser. 3 (1971) 521–547.
[6] M. Lumme, M. Nieminen, J. Peltonen, J.J. Torsti, E. Vainikka, E. Valtonen, Cosmic-ray spectra as calculated from atmospheric hadron cascades, J. Phys. G: Nucl. Part. Phys. 10 (1984) 683–694.
[7] J. Masarik, J. Beer, Simulation of particle fluxes and cosmogenic nuclide production in the Earth's atmosphere, J. Geophys. Res. 104 (1999) 12099–12111.
[8] J. Masarik, J. Beer, An updated simulation of particle fluxes and cosmogenic nuclide production in the Earth's atmosphere, J. Geophys. Res. 114 (2009). CiteID D11103.
[9] J. Masarik, K.J. Kim, R.C. Reedy, Numerical simulations of in situ production of terrestrial cosmogenic nuclides, Nucl. Instrum. Methods Phys. Res., B 259 (2007) 642–645.
[10] J.M. Clem, G. De Angelis, P. Goldhagen, J.W. Wilson, New calculations of the atmospheric cosmic radiation field – results for neutron spectra, Radiat. Prot. Dosim. 110 (2004) 423–428.
[11] T. Sato, K. Niita, Analytical functions to predict cosmic-ray neutron spectra in the atmosphere, Radiat. Res. 166 (2006) 544–555.
[12] T. Sato, H. Yasuda, K. Niita, A. Endo, L. Sihver, Development of PARMA: PHITS-based analytical radiation model in the atmosphere, Radiat. Res. 170 (2008) 244–259.
[13] A.V. Nesterenok, V.O. Naidenov, In situ formation of cosmogenic ^{14}C by cosmic ray nucleons in polar ice, Nucl. Instrum. Methods Phys. Res., B 270 (2012) 12–18.
[14] I.G. Usoskin, G.A. Kovaltsov, Cosmic ray induced ionization in the atmosphere: full modeling and practical applications, J. Geophys. Res. 111 (2006) D21206.
[15] I.G. Usoskin, G.A. Kovaltsov, Production of cosmogenic ^{7}Be isotope in the atmosphere: full 3-D modeling, J. Geophys. Res. 113 (2008) D12107.
[16] G.A. Kovaltsov, I.G. Usoskin, A new 3D numerical model of cosmogenic nuclide ^{10}Be production in the atmosphere, Earth Planet. Sci. Lett. 291 (2010) 182–188.
[17] G.A. Kovaltsov, A. Mishev, I.G. Usoskin, A new model of cosmogenic production of radiocarbon ^{14}C in the atmosphere, Earth Planet. Sci. Lett. 337–338 (2012) 114–120.
[18] A.V. Blinov, Yu.A. Kropotina, Regions of the maximal cosmic ray energy release in the atmosphere, Geomag. Aeron. 49 (2009) 308–314.
[19] S. Agostinelli, J. Allisonas, K. Amakoe, et al., (Geant4 Collaboration), Geant4 – a simulation toolkit, Nucl. Instrum. Methods Phys. Res., A 506 (2003) 250–303.
[20] Geant4 Collaboration, Geant4 physics reference manual [Internet], Available from: <http://geant4.cern.ch/support/index.shtml> (accessed 18.06.12).
[21] R.L. Rudnick, S. Gao, Composition of the continental crust, in: R.L. Rudnick, H.D. Holland, K.K. Turekian (Eds.), Treatise on Geochemistry, Elsevier, 2003, pp. 1–64.
[22] Committee on Space Research (COSPAR), The COSPAR international reference atmosphere (CIRA-86) [Internet], NCAS British Atmospheric Data Centre, Available from: <http://badc.nerc.ac.uk/view/badc.nerc.ac.uk_ATOM_dataent_CIRA> (accessed 18.06.12).
[23] D.F. Smart, M.A. Shea, A review of geomagnetic cutoff rigidities for earth-orbiting spacecraft, Adv. Space Res. 36 (2005) 2012–2020.

[24] D.F. Smart, M.A. Shea, World grid of calculated cosmic ray vertical cutoff rigidities for epoch 1995.0, in: Proceedings of the 30th International Cosmic Ray Conference, vol. 1, 2008, pp. 733–736.
[25] L.I. Dorman, O.A. Danilova, N. Iucci, M. Parisi, N.G. Ptitsyna, M.I. Tyasto, G. Villoresi, Effective non-vertical and apparent cutoff rigidities for a cosmic-ray latitude survey from Antarctica to Italy in minimum of solar activity, Adv. Space Res. 42 (2008) 510–516.
[26] B. Wiebel-Sooth, P.L. Biermann, H. Meyer, Cosmic rays. VII. Individual element spectra: prediction and data, Astron. Astrophys. 330 (1998) 389–398.
[27] K.F. Grieder, Cosmic Rays at Earth, Elsevier, Amsterdam, 2001.
[28] L.J. Gleeson, W.I. Axford, Solar modulation of galactic cosmic rays, Astrophys. J. 154 (1968) 1011–1026.
[29] K. Herbst, A. Kopp, B. Heber, F. Steinhiber, H. Fichtner, K. Scherer, D. Matthia, On the importance of the local interstellar spectrum for the solar modulation parameter, J. Geophys. Res. 115 (2010) D00120.
[30] I.G. Usoskin, K. Alanko-Huotari, G.A. Kovaltsov, K. Mursula, Heliospheric modulation of cosmic rays: monthly reconstruction for 1951–2004, J. Geophys. Res. 110 (2005) A12108.
[31] R.A. Burger, M.S. Potgieter, B. Heber, Rigidity dependence of cosmic ray proton latitudinal gradients measured by the *Ulysses spacecraft*: implications for the diffusion tensor, J. Geophys. Res. 105 (2000) 27447–27456.
[32] I.G. Usoskin, G.A. Bazilevskaya, G.A. Kovaltsov, Solar modulation parameter for cosmic rays since 1936 reconstructed from ground-based neutron monitors and ionization chambers, J. Geophys. Res. 116 (2011) A02104.
[33] A.D. Panov, J.H. Adams, H.S. Ahn, et al., Energy spectra of abundant nuclei of primary cosmic rays from the data of ATIC-2 experiment: final results, Bull. Russ. Acad. Sci.: Phys. 73 (2009) 564–567.
[34] T.J. Dunai, Scaling factors for production rates of in situ produced cosmogenic nuclides: a critical reevaluation, Earth Planet. Sci. Lett. 176 (2000) 157–169.
[35] D. Desilets, M. Zreda, Spatial and temporal distribution of secondary cosmic-ray nucleon intensities and applications to in situ cosmogenic dating, Earth Planet. Sci. Lett. 206 (2003) 21–42.
[36] N.A. Lifton, J.W. Bieber, J.M. Clem, M.L. Duldig, P. Evenson, J.E. Humble, R. Pyle, Addressing solar modulation and long-term uncertainties in scaling secondary cosmic rays for in situ cosmogenic nuclide applications, Earth Planet. Sci. Lett. 239 (2005) 140–161.
[37] J.F. Ziegler, Terrestrial cosmic ray intensities, IBM J. Res. Dev. 42 (1998) 117–139.
[38] M.S. Gordon, P. Goldhagen, K.P. Rodbell, T.H. Zabel, H.H.K. Tang, J.M. Clem, P. Bailey, Measurement of the flux and energy spectrum of cosmic-ray induced neutrons on the ground, IEEE Trans. Nucl. Sci. 51 (2004) 3427–3434.
[39] P. Goldhagen, J.M. Clem, J.W. Wilson, The energy spectrum of cosmic-ray induced neutrons measured on an airplane over a wide range of altitude and latitude, Radiat. Prot. Dosim. 110 (2004) 387–392.
[40] T. Nakamura, T. Nunomiya, S. Abe, K. Terunuma, H. Suzuki, Sequential measurements of cosmic-ray neutron spectrum and dose rate at sea level in Sendai, Japan, J. Nucl. Sci. Technol. 42 (2005) 843–853.
[41] T. Nakamura, Y. Uwamino, T. Ohkubo, A. Hara, Altitude variation of cosmic-ray neutrons, Health Phys. 53 (1987) 509–517.
[42] E. Mochiutti, Atmospheric and Interstellar Cosmic Rays Measured with the CAPRICE98 Experiment, PhD Thesis, Stockholm, 2003, 188 p.